Atmospheric Oxidation Mechanism of 1,2-Dibromoethane†

Carrie J. Christiansen and Joseph S. Francisco*

Department of Chemistry and Department of Earth and Atmospheric Sciences, Purdue University, West Lafayette, Indiana 47909

Received: September 8, 2008; Revised Manuscript Received: October 17, 2008

The complete atmospheric oxidation mechanism of 1,2-dibromoethane is proposed. There are 32 species and 22 transition state species involved in the proposed mechanism. Geometry optimizations and frequency computations are performed using the second-order Møller−Plesset perturbation theory and the 6-31G(d) basis set for all species and transition states. Single-point energy computations are performed using fourth-order Møller−Plesset perturbation theory and coupled cluster theory. Potential energy surfaces, including activation energies and enthalpies, are determined from the computations. Final products of this degradation include OH, CO_2, CO, $CH_2(O)$, CH(O)CH(O) (glyoxal), bromine radicals, CH(O)Br, HOBr, and a reservoir for a new atmospheric compound, BrC(O)C(O)Br.

1. Introduction

The depletion of ozone by halogenated hydrocarbons, particularly choloroflurocarbons (CFCs), is well documented.[1−3] CFCs have significant tropospheric lifetimes, long enough to allow for their transport into the stratosphere. Once there, halogens are released through oxidation and photolysis of the compounds. Halogen radicals catalyze the removal of ozone by converting it to molecular oxygen (reactions 1 and 2).[4]

$$X + O_3 \rightarrow XO + O_2 \quad (1)$$

$$X + O \rightarrow X + O_2 \quad (2)$$

X represents any halogen, including bromine.[5−7] As seen in reactions 1 and 2, a single halogen atom can catalyze the removal of ozone molecules while remaining unchanged, allowing the process to repeat numerous times.

The Montreal Protocol limited the production of a number of ozone depleting compounds, particularly halocarbons.[8,9] In compliance with the agreement, a number of replacements for the banned CFCs have been proposed. Many of these replacements are very short-lived (VSL) compounds. Because of their short lifetimes, VSL compounds are considered acceptable as they are expected to degrade before reaching the stratosphere. However, halogen-containing products produced from the oxidation of these VSL compounds may be long lived and may be transported to the stratosphere. Also, recent studies show that, due to variations in temperature and wind patterns and, therefore, transport times, a number of the VSL compounds may be present in the upper troposphere and lower stratosphere.[10−12]

Brominated compounds are of particular concern. When they reach the stratosphere, bromine atoms catalyze the destruction of ozone 40−50 times more effectively than chlorine atoms.[13−17] In one study of the tropical troposphere and lower stratosphere, 1,2-dibromoethane (EDB) is found to be the most abundant of all the short-lived brominated compounds, at 1.1 ppt of bromine.[11] Its high abundance in the stratosphere, and subsequent ability to destroy ozone, makes EDB of particular concern.

A number of field measurements have been made to determine tropospheric EDB concentrations. Koga et al.[18] measured levels in the air of a remote island of southwest Japan, chosen due to the lack of a local pollution source. They noted a value of 0.007 ppb EDB. Another study assessed the concentrations of a number of aromatic and halogenated hydrocarbons used as additives in gasoline.[19] These measurements, which included dibromoethane, were conducted at three sites (rural, urban, and a busy motorway). For the rural site, dibromoethane had an average concentration of 0.015 parts per thousand million (pptm). Average concentration values at the urban and motorway location were 0.03 and 0.05 pptm, respectively. A study conducted in India measured EDB concentrations at 5.07 μg m^{-3}.[20] Another investigation performed in New Jersey reported a value of 0.03 ppb.[21] Hanwant et al.[22] conducted measurements at four sites in the United States: San Jose, California, Downey, California, Houston, Texas, and Denver, Colorado. They determined mean tropospheric concentrations of 21, 102, 293, and 122 ppt, respectively. Finally, Fischer et al.[23] measured a EDB concentration of 0.1 ppt in the Antarctic air. This value is significant as it is in an unpopulated area and in a location where ozone depletion is of particular concern. EDB is a global problem ranging in concentrations from 0.1 ppt to hundreds of ppt in urban regions.

These high concentrations of EDB are not unanticipated as anthropogenic sources of dibromoethane are numerous and varied. Brominated hydrocarbons, including EDB, are often used as gasoline and oil additives.[24,25] Dibromoethane has also been utilized extensively as a pesticide and fumigant for soil, citrus fruits, and grains.[24,26,27] However, starting in 1983, the EPA limited the pesticide/fumigant uses of EDB due to risks of toxicity. Currently the remaining applications are primarily vault fumigation and quarantine fumigation of nursery stock.[26]

Algae is one of only a few natural sources of bromocarbons and the primary natural source of EDB.[28−31] One study conducted over the Atlantic Ocean showed a correlation between the dibromoethane concentration and the occurrence of brown algae, indicating brown algae as the main contributor of volatilized EDB in the studied regions.[28] It is important to note that EDB undergoes some bacterial degradation in the ocean

† Part of the "Robert Benny Gerber Festschrift".

* To whom correspondence should be addressed. E-mail: francisc@purdue.edu.

10.1021/jp807966p CCC: $40.75
Published on Web 12/31/2008

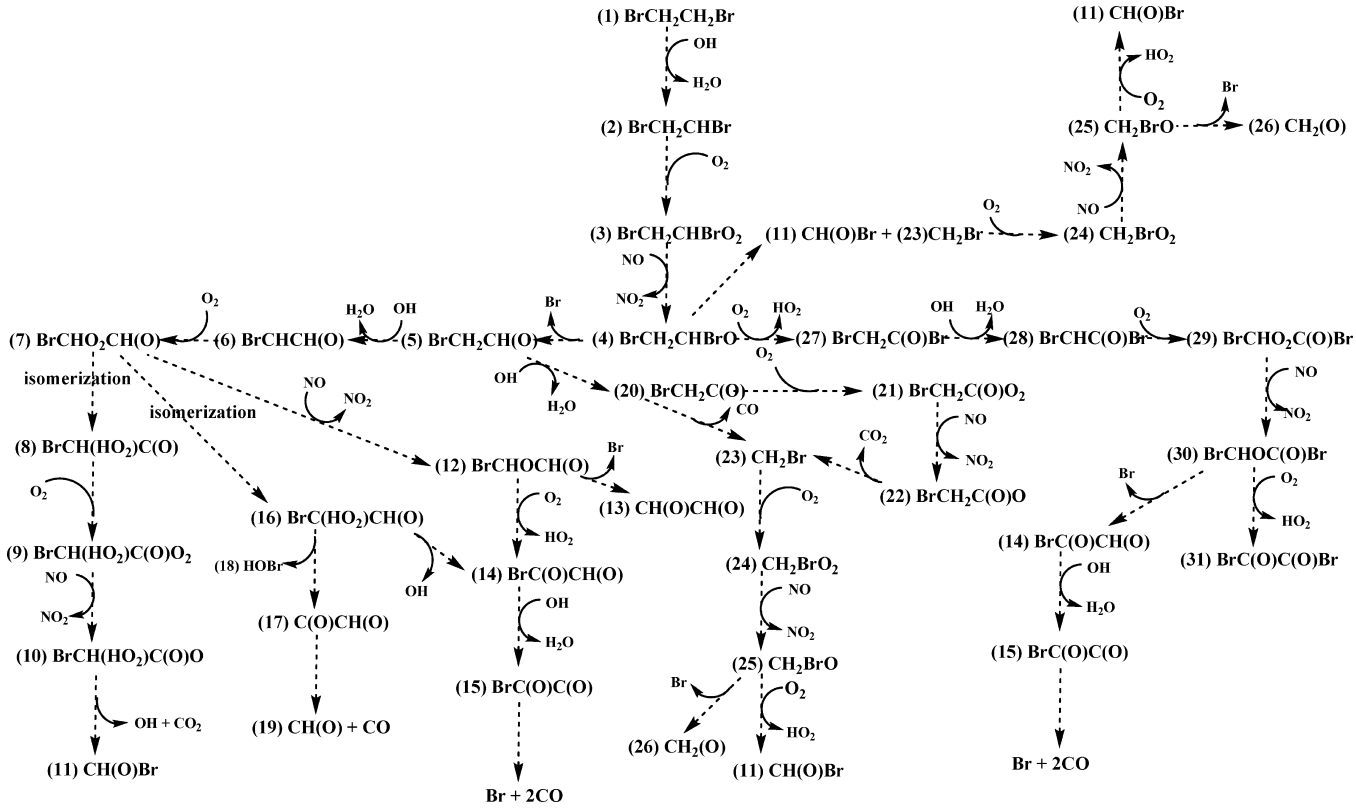

Figure 1. Complete atmospheric degradation mechanism of EDB.

waters. However, this process is minimal when compared to the rate of atmospheric degradation.[32,33]

With a vapor pressure of 11 mmHg and Henry's law constant at 293 K of 3.16×10^{-4} atm m^3 mol^{-1}, EDB volatilizes rapidly from water.[34,35] Therefore, solublized EDB is rapidly released into the gas phase and enters the atmosphere. This is important to note, as the primary natural source of EDB, algae, exists in water. Additionally, with its anthropogenic uses, contamination of ground and surface water is also common.[36]

Dibromoethane has heat of formation values of −37.5 kJ mol^{-1} for the gas phase and −79.2 kJ mol^{-1} for the liquid phase.[37] The boiling point for the compound is 131.6 °C, and the melting point is 9.97 °C.[38]

The gas phase near-infrared spectra of a number of environmentally important gases, including dibromoethane, have been measured.[39] Bose et al. reported infrared spectra for both dibromoethane in an argon matrix at low temperature and in the liquid phase, as well as the Raman spectra for liquid EDB.[40]

To accurately determine the atmospheric impact of dibromoethane, a better understanding of how it degrades in the atmosphere is needed. The atmospheric oxidation of EDB, similar to most organic compounds, begins with the removal of a hydrogen atom by a hydroxyl radical (OH) (reaction 3).

$$(1)\ BrCH_2CH_2Br + OH \rightarrow (2)\ BrCH_2CHBr + H_2O \quad (3)$$

Rate constants for this primary step of the degradation pathway have been determined experimentally. One study reports a value of 2.5×10^{-13} (cm^3 molecule^{-1} s^{-1}).[41] By use of discharge flow and resonance fluorescence, Qiu et al.[42] measured the temperature dependent rate constant as $(14.6 \pm 1.6) \times 10^{-12}\ e^{(-(1281 \pm 136)/T)}$ (cm^3 molecule^{-1} s^{-1}). Calculating the rate constant at 296 K gives $(1.93 \pm 0.39) \times 10^{-13}$ cm^3 molecule^{-1} s^{-1}. From this rate constant, the average temperature of the troposphere, 265 K, and the tropospheric concentration of the hydroxyl radical, 5×10^5 molecules cm^3, the lifetime of EDB in the troposphere is calculated to be 138 days. However the rate constant determined by Qiu et al. is in poor agreement with previously obtained values.[43]

There is no information in the literature concerning the atmospheric oxidative fate of dibromoethane or the resulting byproducts. Consequently, the focus of this work is to investigate the oxidative pathways of dibromoethane computationally.

2. Computational Methods

All computations are performed using the Gaussian 03 suite of programs.[44] Optimized geometries and corresponding energies for reactants, reactive intermediates, products, and transition states are determined using the second-order Møller−Plesset perturbation theory (MP2) with the 6-31G(d) basis set. All electrons are correlated in the MP2 optimization. Frequency computations are also performed with this theory and basis set, giving vibrational mode frequencies, as well as thermochemistry, including the zero point energy (ZPE) correction. The optimized geometries are used to compute single point energies with the following theory and basis set combinations: MP4/6-311++G(2d,2p), MP4/6-311++G(2df,2p), CCSD(T)/6-311++G(2d,2p), CCSD(T)/6-311++G(2df,2p). These energies are corrected with the MP2/6-31G(d) level ZPE correction to obtain total energies. Finally, by use of corrected energies, the enthalpy and activation energy barriers are calculated for individual reactions throughout the degradation pathway steps.

3. Results and Discussion

3.1. Reaction Pathways. The complete atmospheric degradation mechanism of dibromoethane is shown in Figure 1. The complexity of this reaction scheme is broken down into three pathways that are highlighted in parts a−d of Figure 2.

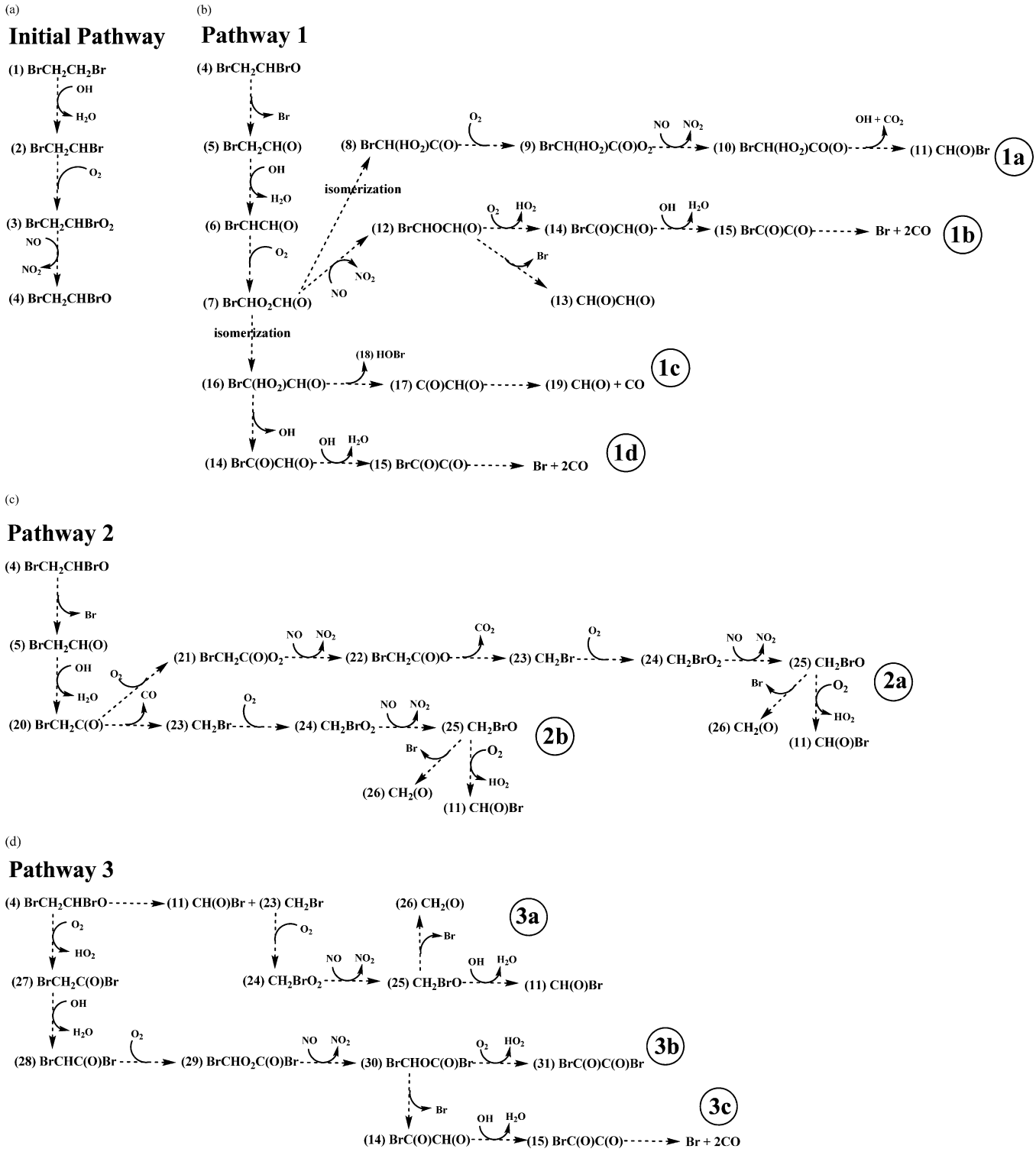

Figure 2. Various pathways in the atmospheric degradation of dibromoethane.

As all hydrogens of EDB are equivalent, the degradation does not contain multiple paths for the initial hydrogen abstraction. Subsequent steps follow: abstraction of the hydrogen, addition of an oxygen molecule to the resulting radical, and subsequent removal of one oxygen atom through a NO/NO_2 conversion (Figure 2a).

The first branch from $BrCH_2CHBrO$ (species 4), pathway 1 (Figure 2b), proceeds with a bromine extrusion, creating $BrCH_2CH(O)$ (species 5). At this point there is another branch; the abstraction of a hydrogen alpha to the bromine continues the degradation along pathway 1, while abstraction of the hydrogen beta to the bromine creates pathway 2. Pathway 1 proceeds to form $BrCHO_2CH(O)$ (species 7), a branching point, containing three possible paths. The first branch, pathway 1a, involves an isomerization of $BrCHO_2CH(O)$ (species 7), finally resulting in another molecule of CH(O)Br (species 11). Pathway 1b progresses from $BrCHO_2CH(O)$ (species 7) with the removal of an oxygen from the peroxy radical. This path results in the following products: a dialdehyde, CH(O)CH(O) (species 13), as well as a bromine radical and carbon monoxide. Pathway 1c also begins with an isomerization of $BrCHO_2CH(O)$ (species 7) to form $BrC(HO_2)CH(O)$ (species 16). Pathway 1c results in

the production of HOBr (species 18) as well as CH(O) (species 19) and carbon monoxide. $BrC(HO_2)CH(O)$ (species 16) can also undergo a hydroxyl radical extrusion creating pathway 1d. This path follows the same steps as pathway 1b and thus results in the same products of a bromine radical and carbon monoxide.

Pathway 2 (Figure 2c) has two branches that eventually result in the same final steps and therefore produce the same products. The $BrCH_2CH(O)$ (species 5) undergoes a hydrogen abstraction to form $BrCH_2C(O)$ (species 20). $BrCH_2C(O)$ (species 20) can proceed on pathway 2a with an O_2 addition followed by an NO/NO_2 conversion removing an oxygen atom, and a CO_2 extrusion to form CH_2Br (species 23). Or $BrCH_2C(O)$ (species 20) can proceed with a CO extrusion to directly form CH_2Br (species 23). The final steps of pathway 2 are also seen in pathway 3a and result in the products of $CH_2(O)$ (species 26) and CH(O)Br (species 11).

Both of the other two branches off of $BrCH_2CHBrO$ (species 4) are grouped as pathway 3 (Figure 2d). Pathway 3a is a fragmentation forming CH_2Br (species 23) and CH(O)Br (species 11). CH_2Br (species 23) continues to be oxidized, ultimately resulting in the products of $CH_2(O)$ (species 26) and another molecule of CH(O)Br (species 11). Pathway 3b involves a hydrogen abstraction from $BrCH_2CHBrO$ (species 4) by O_2 to form $BrCH_2C(O)Br$ (species 27). This oxidation continues along a few more steps, has another branching point, and results in the products of Br radical, carbon monoxide, and BrC(O)C(O)Br (species 31).

3.2. Structures of Species Involved in the Oxidation Mechanism. ***3.2.1. Initial Pathway.*** In the first step of the oxidation, abstraction of a hydrogen, a shift occurs in the geometry from the parent molecule, $BrCH_2CH_2Br$ (species 1, Figure 3a) to $BrCH_2CHBr$ (species 2, Figure 3b). Most noticeable is the change in the angles surrounding the carbon where the hydrogen has been removed. Starting from a tetrahedral like center, with angles ranging from 106.8 to 112.0°, the angles increase, resulting in a geometry close to trigonal planar. These new angles range from 115.6 to 121.6°. The substituents do not achieve full planar characteristic, indicating that a portion of electron density remains on the carbon. This is supported by the Mulliken atomic spin density of 1.171 on that carbon. Additionally, the substituent bond lengths all decrease slightly. The length of the C−Br bond also decreases from 1.960 to 1.875 Å. The transition state associated with this transformation is depicted in Figure 4a.

In the next step, the addition of an O_2 molecule to the radical carbon forms $BrCH_2CHBrO_2$ (species 3, Figure 3c). This O_2 addition reaction pushes the geometry back, similar to that of the parent molecule. The surrounding substituent bond lengths are extended from their lengths in $BrCH_2CHBr$ (species 2) and revert to bond lengths similar to those in the parent molecule. Finally, one oxygen atom from the peroxy radical, $BrCH_2CHBrO_2$ (species 3), is removed through a NO/NO_2 conversion, forming $BrCH_2CHBrO$ (species 4), seen in Figure 3d. This leaves a radical on the oxygen, creating a significantly shorter C−O bond at 1.344 Å. From $BrCH_2CHBrO_2$ (species 3) to $BrCH_2CHBrO$ (species 4), the C−Br length increases from 1.954 to 2.003 Å, while the C−C length increases from 1.504 to 1.520 Å.

From $BrCH_2CHBrO$ (species 4), there are three possible reactions. The first, pathway 1, begins with a bromine extrusion. The other two reactions are contained in pathway 3. Pathway 3a is a fragmentation, and pathway 3b/c begins with a hydrogen abstraction by O_2.

3.2.2. Pathway 1. Pathway 1 begins when $BrCH_2CHBrO$ (species 4) undergoes a bromine extrusion to form $BrCH_2CH(O)$ (species 5, Figure 3e). The transition state of the extrusion is shown in Figure 4b. This structure shows the extension of the C−Br bond, now at a length of 2.217 Å. As this extrusion occurs, the carbon-substituent angles increase from tetrahedral approaching planar. Once the degradation has progressed to $BrCH_2CH(O)$ (species 5) half of the molecule has remained the same as the parent molecule. The other half of the molecule is an aldehyde, with a near trigonal planar geometry. The CCO angle is 122.5°, angle OCH is 122.2°, and angle CCH is 115.3°. The C−C bond is 1.509 Å. A molecule comparable to species 5, $CH_3CH(O)$, has previously been considered computationally.[45] Martínez-Avilés et al. presented the atmospheric oxidation for bromoethane. The geometry presented for $CH_3CH(O)$, optimized at MP2/6-31G(d,p) is quite similar to that obtained for $BrCH_2CH(O)$ (species 5). The CCO angle is 124.3°; angle OCH is 120.3°, and angle CCH is 115.3°. The C−C bond is 1.502 Å. Additionally, the geometry of another comparable molecule, $ClCH_2CH(O)$, is presented by Chandra et al.[46] The CCO angle is 122.6°, and angle CCH is 115.0°. The C−C bond is 1.516 Å. This geometry optimization was performed at MP2/6-311G(d,p) level.

Pathway 1 proceeds from $BrCH_2CH(O)$ (species 5) through a hydrogen abstraction by a hydroxyl radical (Figure 4c) to produce BrCHCH(O) (species 6, Figure 3f). Although a radical remains, this abstraction creates a completely planar molecule with oxygen and bromine atoms in the trans configuration. The Mulliken atomic spin density on the carbon from which the hydrogen was abstracted is 1.090. This value indicates that, although the geometry surrounding the carbon is planar, the radical is centered on that carbon. The π system created by the carbon−oxygen double bond on the adjacent carbon may explain the planar geometry. As with the previous hydrogen abstraction, this step is followed by an O_2 addition. The addition creates $BrCHO_2CH(O)$ (species 7, Figure 3g). As before, a restoration of geometry occurs, similar to $BrCH_2CH(O)$ (species 5).

At this point, there are a myriad of possible paths. These pathways are now differentiated as pathway 1a, pathway 1b, and pathway 1c/d. In pathway 1a, $BrCHO_2CH(O)$ (species 7) is converted to $BrCH(HO_2)C(O)$ (species 8, Figure 3h). This transition occurs through an isomerization in which the O_2 substituent removes a hydrogen from the neighboring carbon to produce a hydroperoxide. As seen in Figure 4d, the transition state is composed of a five-member ring consisting of both carbons, both oxygens, and the hydrogen. The resulting geometry differs significantly from that of $BrCHO_2CH(O)$ (species 7) as the move of the hydrogen shifts the location of the radical. In $BrCHO_2CH(O)$ (species 7) the radical resides as a peroxy radical, but in $BrCH(HO_2)C(O)$ (species 8), it is now located on the neighboring carbon. This shift of the radical increases the length of the O−O bond from 1.320 to 1.476 Å. The geometry of the new radical carbon does not change significantly; it remains trigonal planar, with a radical positioned where the hydrogen was previously. $BrCH(HO_2)C(O)$ (species 8) now undergoes O_2 addition into the radical carbon forming $BrCH(HO_2)C(O)O_2$ (species 9, Figure 3i). Following this addition, the peroxy radical is reduced to an alkoxy radical through a NO/NO_2 conversion to produce $BrCH(HO_2)C(O)O$ (species 10, Figure 3j). Finally, this species undergoes fragmentation to produce three products: OH, CO_2, and CH(O)Br (species 11, Figure 3k). CH(O)Br (species 11) has been previously considered computationally, and the geometry and energy for the species are given in the literature.[45] The analogous

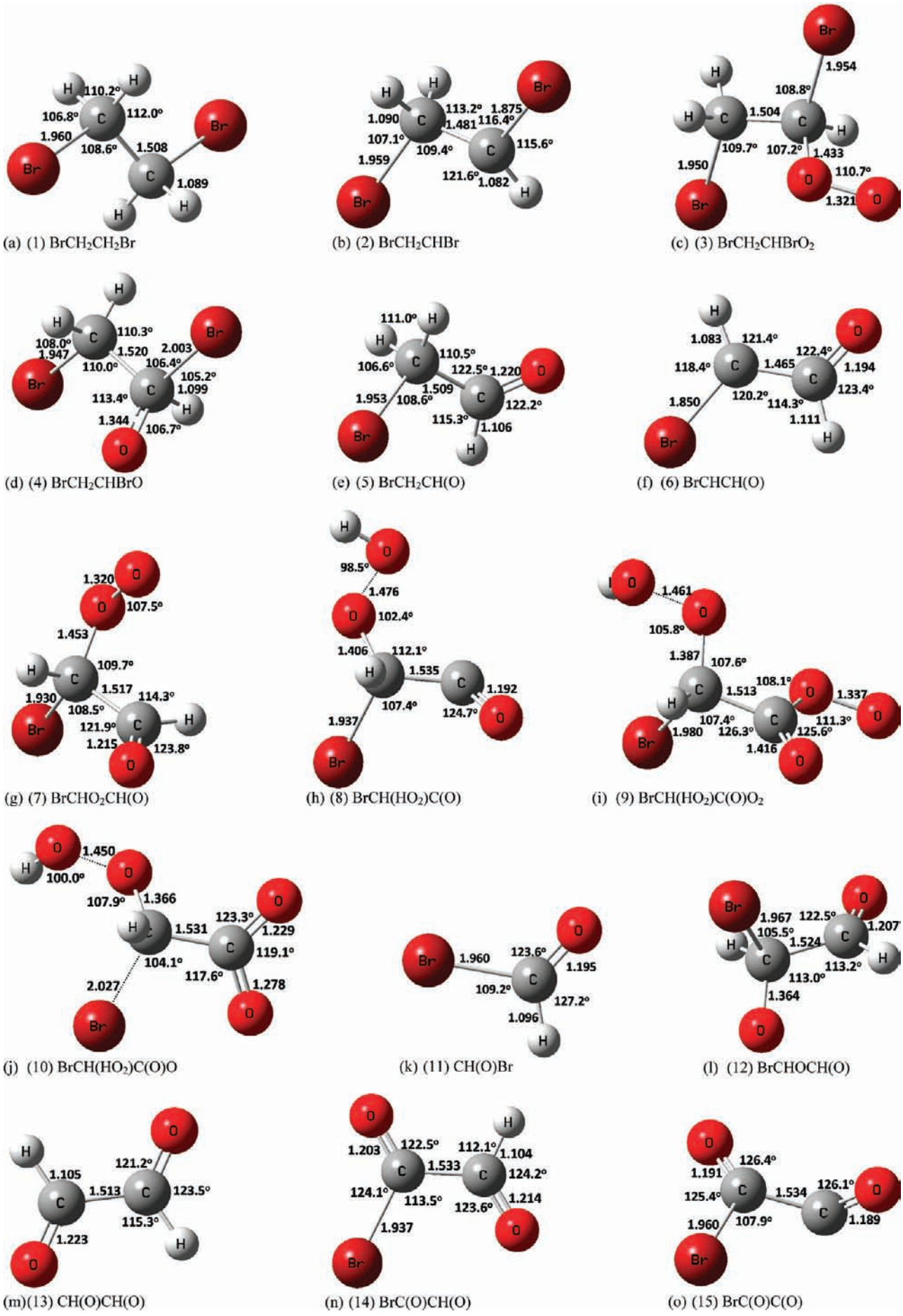

Figure 3. Part 1 of 2.

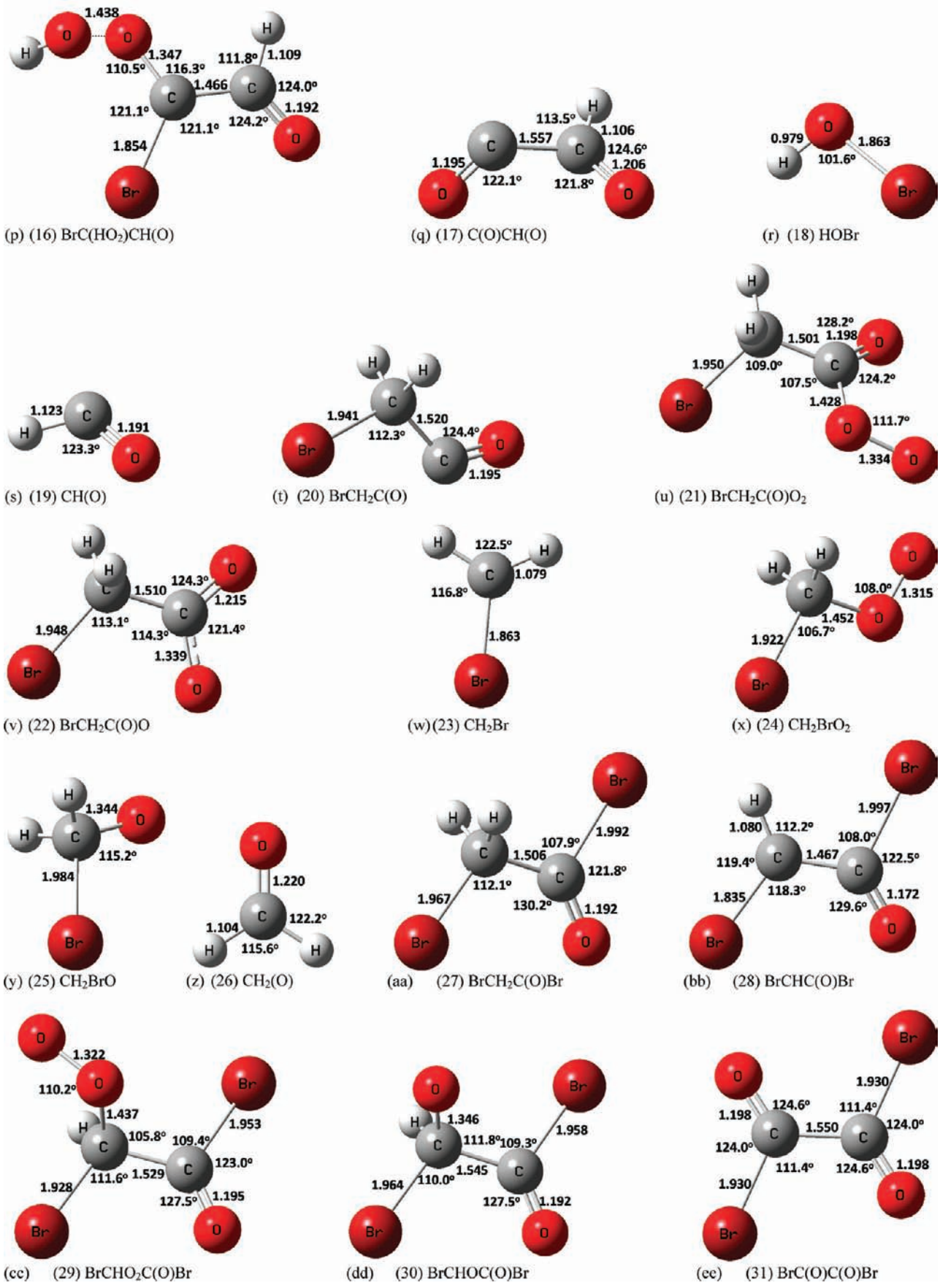

Figure 3. Part 2 of 2. Structures of reactants, reactive intermediates, and products. Bond distances are given in angstroms and angles in degrees.

molecule, where bromine is substituted with a hydrogen atom is also presented in the aforementioned publication. The bromine affects the geometry significantly. CH(O)Br (species 11) has the following angles: angle OCH is 127.2°; angle OCBr is

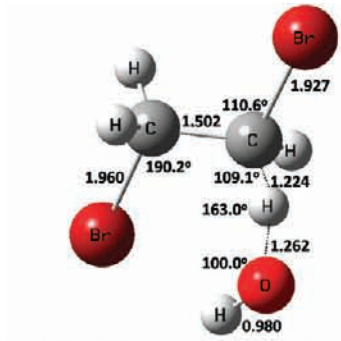

(a) [(1) $BrCH_2CH_2Br + OH \rightarrow$ (2) $BrCH_2CHBr + H_2O$]‡, TS 1-2

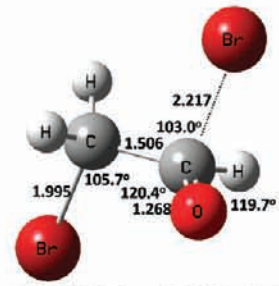

(b) [(4) $BrCH_2CHBrO \rightarrow$ (5) $BrCH_2CH(O) + Br$]‡, TS 4-5

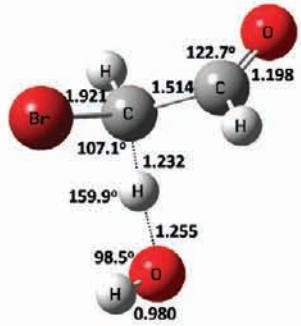

(c) [(5) $BrCH_2CH(O) + OH \rightarrow$ (6) $BrCHCH(O) + H_2O$]‡, TS 5-6

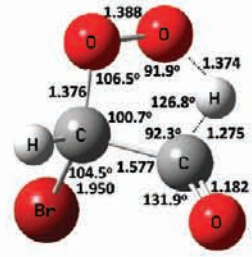

(d) [(7) $BrCHO_2CH(O) \rightarrow$ (8) $BrCH(HO_2)C(O)$]‡, TS 7-8

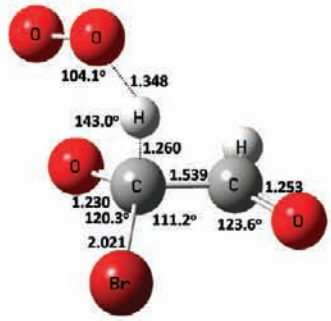

(e) [(12) $BrCHOCH(O) + O_2 \rightarrow$ (14) $BrC(O)CH(O) + HO_2$]‡, TS 12-14

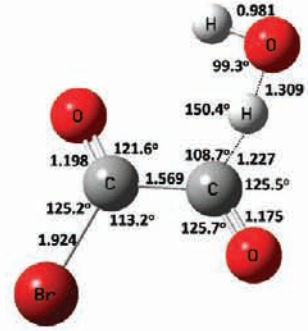

(f) [(14) $BrC(O)CH(O) + OH \rightarrow$ (15) $BrC(O)C(O) + H_2O$]‡, TS 14-15

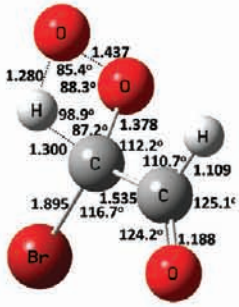

(g) [(7) $BrCHO_2CH(O) \rightarrow$ (16) $BrC(HO_2)CH(O)$]‡, TS 7-16

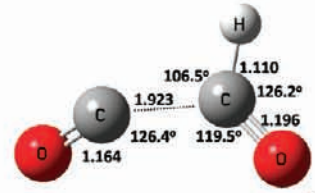

(h) [(17) $C(O)CH(O) \rightarrow$ (19) $CH(O) + CO$]‡, TS 17-19

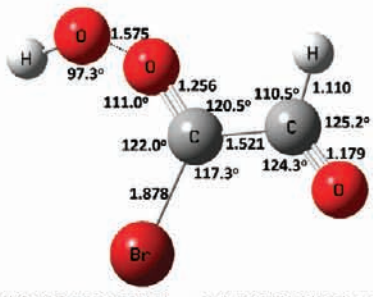

(i) [(16) $BrC(HO_2)CH(O) \rightarrow$ (14) $BrC(O)CH(O) + OH$]‡, TS 16-14

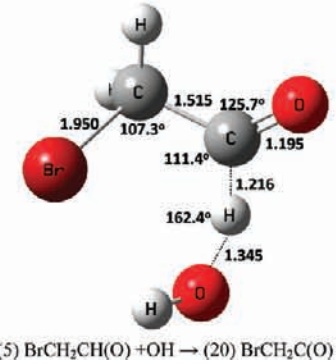

(j) [(5) $BrCH_2CH(O) + OH \rightarrow$ (20) $BrCH_2C(O) + H_2O$]‡, TS 5-20

Figure 4. Part 1 of 2.

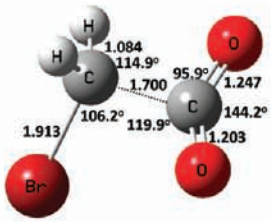

(k) [(22) $BrCH_2C(O)O \rightarrow$ (23) $CH_2Br + CO_2$]‡, TS 22-23

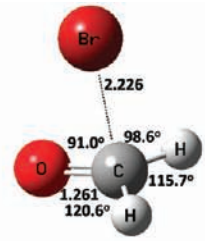

(l) [(25) $CH_2BrO \rightarrow$ (26) $CH_2(O) + Br$]‡, TS 25-26

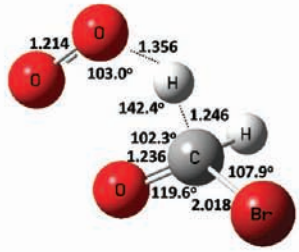

(m)[(25) $CH_2BrO + O_2 \rightarrow$ (11) $CH(O)Br + HO_2$]‡, TS 25-11

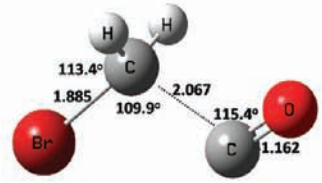

(n) [(20) $BrCH_2C(O) \rightarrow$ (23) $CH_2Br + CO$]‡, TS 20-23

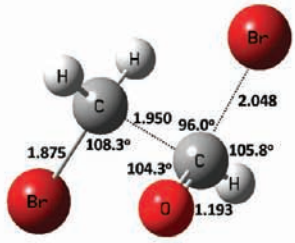

(o) [(4) $BrCH_2CHBrO \rightarrow$ (11) $CH(O)Br$ + (23) CH_2Br]‡, TS 4-23

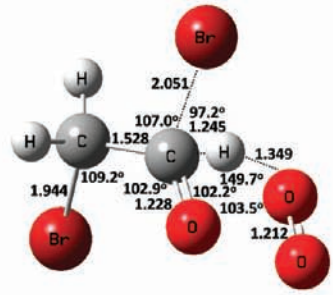

(p) [(4) $BrCH_2CHBrO + O_2 \rightarrow$ (27) $BrCH_2C(O)Br + HO_2$]‡, TS 4-27

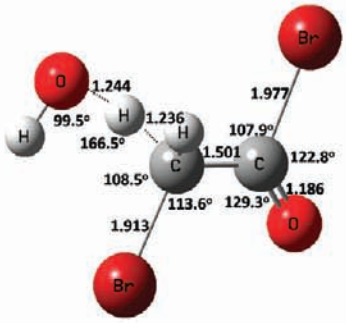

(q) [(27) $BrCH_2C(O)Br + OH \rightarrow$ (28) $BrCHC(O)Br + H_2O$]‡, TS 27-28

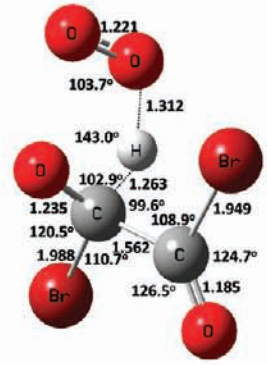

(r) [(30) $BrCHOC(O)Br + O_2 \rightarrow$ (31) $BrC(O)C(O)Br + HO_2$]‡, TS 30-31

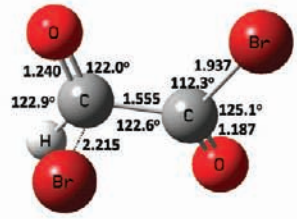

(s) [(30) $BrCHOC(O)Br \rightarrow$ (14) $BrC(O)CH(O) + Br$]‡, TS 30-14

Figure 4. Part 2 of 2. Transition-state structures. Bond distances are given in angstroms and angles in degrees.

123.6°; angle HCBr is 109.2°. Whereas CH(O)H has the following angles: both OCH angles are 122.2°, and angle HCH is 115.6°. The CO bond length is 1.195 Å for CH(O)Br (species 11) but 1.220 Å for CH(O)H.

Pathway 1b begins with the removal of an oxygen atom through a NO/NO_2 conversion to form BrCHOCH(O) (species 12, Figure 3l). The C−C bond increases from 1.517 to 1.524 Å, and the C−Br bond increases from 1.930 to 1.967 Å. BrCHOCH(O) (species 12) then proceeds in two directions. First, a bromine extrusion creates CH(O)CH(O) (species 13), glyoxal, a planar trans-dialdehyde, a final product of the EDB degradation (Figure 3m). It has a C−C bond length of 1.513

Å, a C−O bond length of 1.223 Å, and a C−H bond length of 1.105 Å. The angles in the molecule are as follows: angle CCO is 121.2°, and angle CCH is 115.3°. This compound has been studied extensively both computationally and experimentally. One study calculates the ground-state geometry and energies of glyoxal using the 6-31G(d,p) basis set with a number of theories.[47] The HF computed bond lengths and angles are close to those listed here with slight differences. This product is of particular importance due to its ability to contribute to secondary organic aerosols formation.[48,49] Photolysis data for glyoxal is given in the literature.[50]

The other possible path for BrCHOCH(O) (species 12) is a hydrogen abstraction by molecular oxygen. The transition state structure is shown in Figure 4e. This process produces an HO_2 radical as well as BrC(O)CH(O) (species 14, Figure 3n), a planar aldehyde with trans oxygens. This closed shell system subsequently undergoes another hydrogen abstraction, this time by a hydroxyl radical (see Figure 4f for transition state) to form BrC(O)C(O) (species 15, Figure 3o). The Mulliken atomic spin densities for BrC(O)C(O) (species 15) indicate a slight distribution of the radical electron. The spin density for the carbon from which the hydrogen was abstracted is 0.647. This value signifies a majority of the electron density is localized on the carbon, explaining the trigonal planar geometry around this carbon. However, a significant portion, 0.193, of the spin density is located on the α oxygen. As an end to this pathway, the destabilizing effect of the radical helps to push the two carbons apart and leads to the fragmentation of the molecule to create two carbon monoxide molecules and a bromine radical.

Pathway 1c also breaks from the other paths at $BrCHO_2CH(O)$ (species 7). As in pathway 1a, this transition occurs through an isomerization. Again, the peroxy radical removes a hydrogen; however, this hydrogen is removed from the same carbon to which the peroxy radical is bonded. As such, the transition state of this isomerization is a four-membered ring (Figure 4g). This process creates $BrC(HO_2)CH(O)$ (species 16, Figure 3p). The hydrogen removal creates a radical carbon. The additional electron density is localized on the carbon, shown by a Mulliken atomic spin density of 0.976; however, the geometry remains planar. From $BrCHO_2CH(O)$ (species 7) to $BrC(HO_2)CH(O)$ (species 16), the C−C bond length decreases from 1.517 to 1.466 Å; the C−Br bond length decreases from 1.930 to 1.854 Å; the C−O bond length changes from 1.453 to 1.347 Å. Next, $BrC(HO_2)CH(O)$ (species 16) undergoes an unusual fragmentation. HOBr (species 18, Figure 3r), a final product, is formed from the bromine and the hydrogen and oxygen on the hydroperoxide group, leaving C(O)CH(O) (species 17) (Figure 2q). The final step in pathway 1c is the fragmentation of C(O)CH(O) (species 17) to carbon monoxide and the radical aldehyde product, CH(O) (species 19, Figure 3s). This fragmentation occurs with a transition state C−C bond length of 1.923 Å (Figure 4h).

Pathway 1d branches off pathway 1c at $BrC(HO_2)CH(O)$ (species 16). Figure 4i shows the transition from $BrC(HO_2)CH(O)$ (species 16) to BrC(O)CH(O) (species 14) through an OH extrusion. This transition structure shows an O−O bond length of 1.575 Å. After formation of BrC(O)CH(O) (species 14), pathway 1d continues along the same path as that of 1b.

3.2.3. Pathway 2. Pathway 2 diverges at $BrCH_2CH(O)$ (species 5). Pathway 2 involves the removal of the hydrogen beta to the remaining bromine. This abstraction results in $BrCH_2C(O)$ (species 20, Figure 3t), through the transition state illustrated in Figure 4j. The CCO angle is still in the trigonal planar form at 124.4° although slightly increased from the previous angle of 122.5°. From $BrCH_2C(O)$ (species 20), there are two possible paths, both converging on the same final course. Pathway 2a progresses with the oxidation of $BrCH_2C(O)$ (species 20) by the addition of O_2 into the carbon centered radical. This forms $BrCH_2C(O)O_2$ (species 21). As shown in Figure 3u, this structure has a tetrahedral geometry on one end of the molecule and a trigonal planar geometry on the opposite end. The two ends are partially eclipsed but with the alignment of the hydrogen and the alkoxy radical. As in most other cases, this peroxy radical is reduced by NO to $BrCH_2C(O)O$ (species 22, Figure 3v). After this reduction, a fragmentation occurs to produce CO_2 and CH_2Br (species 23, Figure 3w). The associated transition state shows a C−C bond length of 1.700 Å (Figure 4k). The longer of the two C−O bonds decreases from 1.339 to 1.203 Å, verging closer to the C−O length of CO_2, 1.179 Å. Along with the decrease in bond length, an increase of both CCO angles occurs, creating an OCO angle closer to the 180° seen in CO_2. Next, CH_2Br (species 23) undergoes an O_2 addition and subsequent reduction to form CH_2BrO_2 (species 24, Figure 3x) and CH_2BrO respectively (species 25, Figure 3y). Geometries are computed for species comparable to CH_2BrO_2 (species 24) and CH_2BrO (species 25), where the bromine is substituted with a hydrogen atom, and are available in the literature.[45] From CH_2BrO (species 25) there are two paths. The first involves a bromine extrusion through the transition state depicted in Figure 4l to produce formaldehyde, $CH_2(O)$ (species 26, Figure 3z). Second is a hydrogen abstraction to produce CH(O)Br, the brominated aldehyde (species 11, Figure 3k). This product is also formed at the end of pathway 1a. The transition state geometry for this reaction can be seen in Figure 4m.

Pathway 2b involves the fragmentation of $BrCH_2C(O)$ (species 20) to produce a CO molecule and CH_2Br (species 23). This fragmentation has a transition state C−C bond length of 2.067 Å as seen in Figure 4n. After the fragmentation and production of CH_2Br (species 23), pathway 2b follows the identical progression as that of 2a.

3.2.4. Pathway 3. Pathway 3 encompasses two branches off of $BrCH_2CHBrO$ (species 4). The first pathway, 3a, begins as $BrCH_2CHBrO$ (species 4) undergoes a fragmentation and results in additional sources of both CH(O)Br (species 11) and CH_2Br (species 23). Figure 4o shows the transition structure, with a C−C bond length of 1.950 Å. CH_2Br (species 23) then continues along the same oxidation path as that in pathway 2.

The other two portions of pathway 3, 3b and 3c, progress along the same path for a number of steps, starting with a hydrogen abstraction from $BrCH_2CHBrO$ (species 4), forming $BrCH_2C(O)Br$ (species 27, Figure 3aa). The geometry for a molecule comparable to $BrCH_2C(O)Br$ (species 27), $CH_3C(O)Br$, has been optimized at the MP2/6-31G(d,p) level.[45] According to the computations, these two molecules have close geometries. The BrCO angle on $BrCH_2C(O)Br$ (species 27) is 1.3° larger than that on $CH_3C(O)Br$. Additionally, the CH_3 group on $CH_3C(O)Br$ maintains an almost exact tetrahedral geometry, while the $BrCH_2$ group on $BrCH_2C(O)Br$ (species 27) has an increased CCBr angle of 112.1°. Figure 4p depicts the geometry of the transition structure of the reaction converting $BrCH_2CHBrO$ (species 4) to $BrCH_2C(O)Br$ (species 27). The bond angles of the substituents surrounding the radical carbon increase, adopting a trigonal planar geometry. The radical produced from the hydrogen abstraction is paired with the alkoxy radical, forming a stronger bond with a length similar to that of a double C−O bond; dropping from 1.344 to 1.192 Å. Immediately following this abstraction, converting $BrCH_2$-

CHBrO (species 4) to $BrCH_2C(O)Br$ (species 27), another hydrogen abstraction occurs, converting $BrCH_2C(O)Br$ (species 27) to BrCHC(O)Br (species 28). BrCHC(O)Br (species 28) is a fully planar molecule with trans bromine atoms (Figure 3bb). For the transition structure of the $BrCH_2C(O)Br$ (species 27) to BrCHC(O)Br (species 28) reaction, see Figure 4q. As with a number of hydrogen abstractions, the addition of O_2 follows to produce a peroxy radical, $BrCHO_2C(O)Br$ (species 29, Figure 3cc). A reaction with NO reduces the peroxy to an alkoxy radical and creates BrCHOC(O)Br (species 30, Figure 3dd). As the radical is repositioned, the electron density spreads into the C−O bond decreasing its length from 1.437 to 1.346 Å. BrCHOC(O)Br (species 30) is where pathways 3b and 3c diverge. Pathway 3b ends with a hydrogen abstraction from BrCHOC(O)Br (species 30) to form BrC(O)C(O)Br (species 31, Figure 3ee). The transition structure for this reaction can be seen in Figure 4r. BrC(O)C(O)Br (species 31) is analogous to CH(O)CH(O) (species 13), glyoxal. BrC(O)C(O)Br (species 31) has a C−C bond length of 1.550 Å, a C−O bond length of 1.198 Å, and a C−Br bond length of 1.930 Å. The CCO angle is 124.6°, and the CCBr angle is 111.4°. Glyoxal has a C−C bond length of 1.513 Å, a C−O bond length of 1.223 Å, and a C−H bond length of 1.105 Å. The angles in the molecule are as follows: angle CCO is 121.2°, and angle CCH is 115.3°. As discussed, glyoxal is thought to contribute to secondary organic aerosols formation. With the similar structure, BrC(O)C(O)Br (species 31) may also play a role in aerosol formation. However, as much of the aerosol formation results from hydrogen bonding, the bromines may limit the ability of BrC(O)C(O)Br (species 31) to contribute to aerosol formation.

Pathway 3c converts BrCHOC(O)Br (species 30) into BrC(O)CH(O) (species 14) through a bromine extrusion. The associated transition state is given in Figure 4s. The progression from BrC(O)CH(O) (species 14) continues as that given in pathway 1b.

3.3. Oxidation Mechanism Energetics. By use of calculated enthalpies and activation energies, the potential energy surfaces for the atmospheric degradation of dibromoethane are shown in parts a−d of Figure 5. These surfaces allow for a visual description of the energy barriers as well as the overall thermodynamic driving forces for diverging pathways.

By use of the zero point corrected energies for all species, enthalpies for all reactions involved in the degradation are calculated and are given in Table 1. Table 2 shows activation energies for selected reactions in the degradation pathways. Zero point corrected energies of reactants, reactive intermediates, and products are available in Table 1 of Supporting Information. Table 2 of Supporting Information contains zero point corrected energies of the transition states. The vibrational frequencies for reactants, reactive intermediates, products, and transition states are given in Tables 3 and 4 of Supporting Information, respectively.

Comparison of the enthalpies and activation energies calculated from energies computed at MP4/6-311++G(2df,2p) with those computed at CCSD(T)/6-311++G(2df,2p) show a good convergence. However, there are a number of reaction ethalpies that do not converge well between the two theory levels. Primarily, this poor convergence occurs in reactions where a peroxy radical is reduced to an alkoxy radical through an NO/NO_2 conversion. For the enthalpies, the root-mean-square value of the difference between the two methods is 3.9 kcal mol^{-1}. Excluding the NO/NO_2 conversion reactions, the root-mean-square value is lowered to 2.8 kcal mol^{-1}. For the activation energy, the root-mean-square value of the difference between the two methods is 2.9 kcal mol^{-1}.

3.3.1. Initial Pathway. The initial four steps of the degradation are given in Figure 5a. The first reaction, from $BrCH_2CH_2Br$ (species 1) to $BrCH_2CHBr$ (species 2), corresponds to a hydrogen abstraction by OH radical and is depicted in reaction 3

$$(1)\ BrCH_2CH_2Br + OH \rightarrow (2)\ BrCH_2CHBr + H_2O\ (3)$$

The energy barrier for this reaction is 1.9 kcal mol^{-1} and has an enthalpy of −17.5 kcal mol^{-1}. The saddle point is identified by an imaginary frequency corresponding to the C−H−O vibration and has a value of 2400*i* cm^{-1}. The resulting $BrCH_2CHBr$ radical can undergo an addition with O_2 (reaction 4). Followed by its formation, the peroxy radical is then oxidized by NO (reaction 5)

$$(2)\ BrCH_2CHBr + O_2 \rightarrow (3)\ BrCH_2CHO_2Br \quad (4)$$

$$(3)\ BrCH_2CHO_2Br + NO \rightarrow (4)\ BrCH_2CHOBr + NO_2 \quad (5)$$

Reaction 4 has an enthalpy of −28.6 kcal mol^{-1}, corresponding to the release of energy associated with the formation of the C−O bond. Reaction 5 represents the reduction of the peroxy radical $BrCH_2CHBrO_2$ (species 3) through an NO/NO_2 conversion to form $BrCH_2CHBrO$ (species 4). The enthalpy for this reaction is −15.6 kcal mol^{-1}.

The $BrCH_2CHOBr$ alkoxy radical has three possible reactions as shown below (reactions 6−8)

$$(4)\ BrCH_2CHOBr \rightarrow (5)\ BrCH_2COH + Br \quad (6)$$

$$(4)\ BrCH_2CHOBr \rightarrow (11)\ CH(O)Br + (23)\ CH_2Br \quad (7)$$

$$(4)\ BrCH_2CHOBr + O_2 \rightarrow (27)\ BrCH_2COBr + HO_2 \quad (8)$$

Reaction 6 is the unimolecular release of the first bromine atom. This reaction has an activation energy of −0.9 kcal mol^{-1} with the saddle point having an imaginary frequency of 619*i* cm^{-1} and corresponds with the C−Br vibration. The slightly negative activation energy suggests that within the uncertainties of these computations there is no activation energy barrier for this process. The enthalpy of this extrusion is −10.8 kcal mol^{-1}, associated with the breaking of the C−Br bond and formation of the C−O double bond.

Reaction 7 represents a C−C bond fission process. This unimolecular fragmentation results in the formation of one product, CH(O)Br (species 11), a radical bromomethane, and a reactive intermediate, CH_2Br, a brominated aldehyde (species 23). The activation energy required for this reaction is 11.3 kcal mol^{-1}. This transition state has a frequency of 776*i* cm^{-1} corresponding to the C−C vibration. The enthalpy for this reaction is 0.5 kcal mol^{-1}.

Given the significant abundance of O_2 in the atmosphere, hydrogen abstraction from the $BrCH_2CHOBr$ alkoxy radical by O_2 can occur as described in reaction 8. The energy barrier for this reaction is 0.5 kcal mol^{-1} and has a negative vibrational frequency of 1080*i* cm^{-1}. The associated enthalpy is −37.3 kcal mol^{-1}.

3.3.2. Pathway 1. The potential energy surface for pathway 1 is shown in Figure 5b. It begins with the bromine extrusion from $BrCH_2CHBrO$ (species 4), forming $BrCH_2CH(O)$ (species 5), as discussed in the previous section. The degradation proceeds from $BrCH_2CH(O)$ (species 5) through a hydrogen abstraction followed by an O_2 addition to produce $BrCHO_2CH(O)$ (species 7), the splitting point for pathways 1a−d. Reactions 9−11 are the possible directions that $BrCHO_2CH(O)$ (species 7) can proceed.

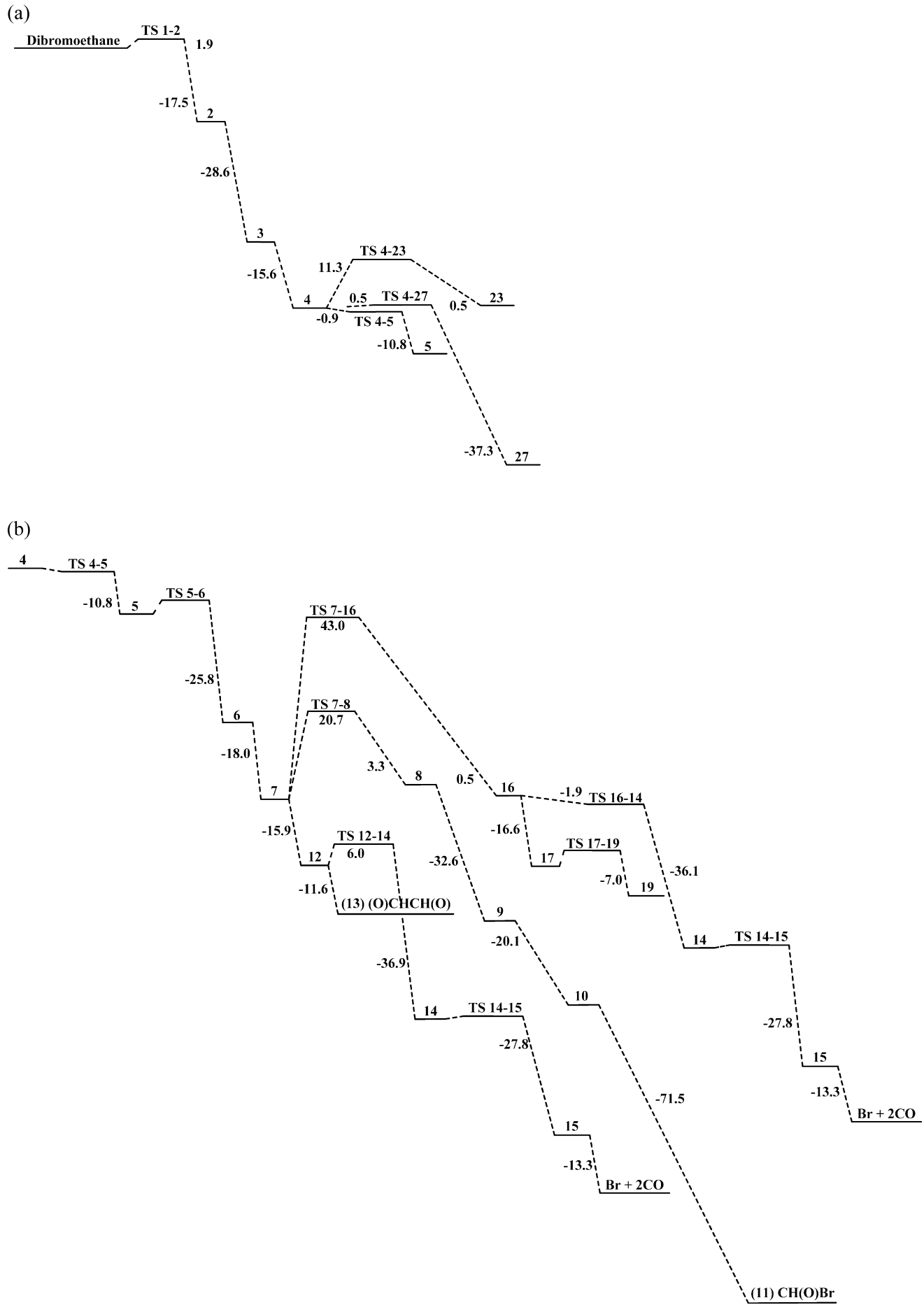

Figure 5. Part 1 of 2.

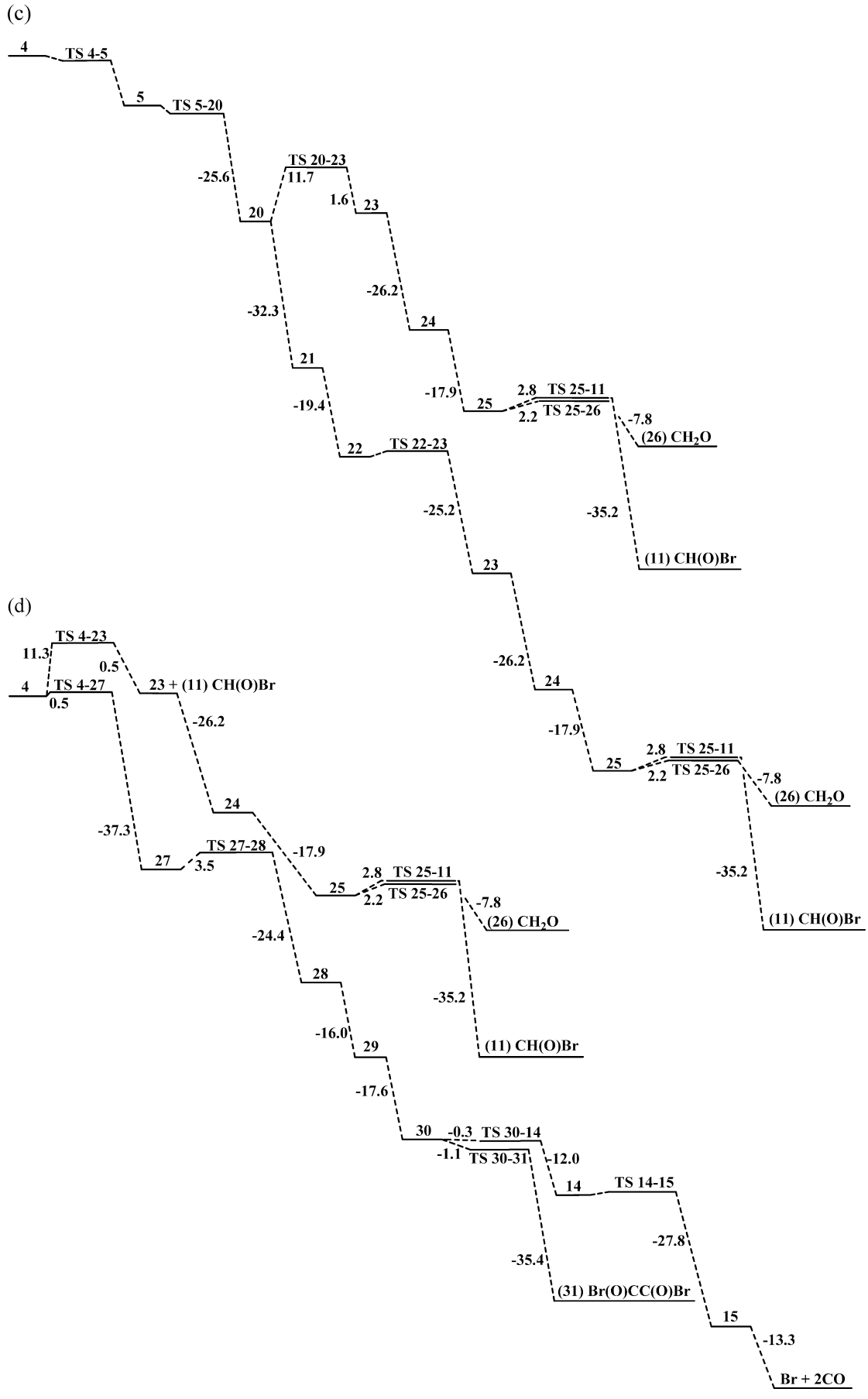

Figure 5. Part 2 of 2. Potential energy surface of degradation pathways. Energy units in kcal mol^{-1}.

TABLE 1: Enthalpy for Oxidation Reactions of 1,2-Dibromoethane (kcal mol^{-1}) (Values Corrected with Zero Point Energy)

reaction	MP2 6-31G(d)	MP4 6-311++G (2d,2p)	MP4 6-311++G (2df,2p)	CCSD(T) 6-311++G (2d,2p)	CCSD(T) 6-311++G (2df,2p)
Initial Pathway					
(1) $BrCH_2CH_2Br + OH \rightarrow$ (2) $BrCH_2CHBr + H_2O$	−11.6	−16.8	−17.6	−16.7	−17.5
(2) $BrCH_2CHBr + O_2 \rightarrow$ (3) $BrCH_2CHBrO_2$	−21.8	−23.8	−26.1	−26.5	−28.6
(3) $BrCH_2CHBrO_2 + NO \rightarrow$ (4) $BrCH_2CHBrO + NO_2$	−23.8	−22.6	−23.4	−14.8	−15.6
Pathway 1a					
(4) $BrCH_2CHBrO \rightarrow$ (5) $BrCH_2CH(O) + Br$	−11.8	−14.4	−13.3	−11.6	−10.8
(5) $BrCH_2CH(O) + OH \rightarrow$ (6) $BrCHCH(O) + H_2O$	−13.6	−21.2	−22.0	−24.9	−25.8
(6) $BrCHCH(O) + O_2 \rightarrow$ (7) $BrCHO_2CH(O)$	−16.7	−16.9	−19.1	−15.9	−18.0
(7) $BrCHO_2CH(O) \rightarrow$ (8) $BrCH(HO_2)C(O)$	1.2	−0.8	−0.1	2.5	3.3
(8) $BrCH(HO_2)C(O) + O_2 \rightarrow$ (9) $BrCH(HO_2)C(O)O_2$	−26.1	−26.7	−29.6	−29.9	−32.6
(9) $BrCH(HO_2)C(O)O_2 + NO \rightarrow$ (10) $BrCH(HO_2)C(O)O$[a] $+ NO_2$		−23.1	−24.4	−19.1	−20.1
(10) $BrCH(HO_2)C(O)O \rightarrow$ (11) $CH(O)Br + CO_2 + OH$[a]		−81.7	−79.8	−73.0	−71.5
Pathway 1b					
(7) $BrCHO_2CH(O) + NO \rightarrow$ (12) $BrCHOCH(O) + NO_2$	−22.3	−22.0	−22.9	−15.1	−15.9
(12) $BrCHOCH(O) \rightarrow$ (13) $CH(O)CH(O) + Br$	−16.1	−16.1	−14.9	−12.6	−11.6
(12) $BrCHOCH(O) + O_2 \rightarrow$ (14) $BrC(O)CH(O) + HO_2$	−32.4	−37.9	−38.4	−36.3	−36.9
(14) $BrC(O)CH(O) + OH \rightarrow$ (15) $BrC(O)C(O) + H_2O$	−22.9	−29.4	−29.5	−27.6	−27.8
(15) $BrC(O)C(O) \rightarrow$ $2CO + Br$	−11.3	−18.5	−12.5	−18.8	−13.3
Pathway 1c					
(7) $BrCHO_2CH(O) \rightarrow$ (16) $BrC(HO_2)CH(O)$	7.1	3.3	2.8	0.9	0.5
(16) $BrC(HO_2)CH(O) \rightarrow$ (17) $C(O)CH(O)$ + (18) HOBr	−22.1	−25.0	−23.1	−18.2	−16.6
(17) $C(O)CH(O) \rightarrow$ (19) $CH(O) + CO$	−8.4	−11.2	−7.1	−9.7	−7.0
Pathway 1d (See 1b ΔH)					
(16) $BrC(HO_2)CH(O) \rightarrow$ (14) $BrC(O)CH(O) + OH$	−46.1	−45.8	−42.6	−39.3	−36.1
Pathway 2a					
(4) $BrCH_2CHBrO \rightarrow$ (5) $BrCH_2CH(O) + Br$	−11.8	−14.4	−13.3	−11.6	−10.8
(5) $BrCH_2CH(O) + OH \rightarrow$ (20) $BrCH_2C(O) + H_2O$	−21.9	−26.8	−26.9	−25.4	−25.6
(20) $BrCH_2C(O) + O_2 \rightarrow$ (21) $BrCH_2C(O)O_2$	−24.4	−26.2	−29.1	−29.5	−32.3
(21) $BrCH_2C(O)O_2 + NO \rightarrow$ (22) $BrCH_2C(O)O + NO_2$	−26.0	−25.4	−26.5	−18.5	−19.4
(22) $BrCH_2C(O)O \rightarrow$ (23) $CH_2Br + CO_2$	−29.5	−28.9	−29.5	−24.3	−25.2
(23) $CH_2Br + O_2 \rightarrow$ (24) CH_2BrO_2	−17.8	−20.7	−23.2	−23.9	−26.2
(24) $CH_2BrO_2 + NO \rightarrow$ (25) $CH_2BrO + NO_2$	−26.9	−25.2	−26.0	−17.2	−17.9
(25) $CH_2BrO \rightarrow$ (26) $CH_2(O) + Br$	−10.1	−11.6	−10.3	−8.8	−7.8
(25) $CH_2BrO + O_2 \rightarrow$ (11) $CH(O)Br + HO_2$	−27.2	−34.6	−35.4	−34.4	−35.2
Pathway 2b (See 2a ΔH)					
(20) $BrCH_2C(O) \rightarrow$ (23) $CH_2Br + CO$	5.0	0.3	2.8	0.0	2.3
Pathway 3a (See 2a ΔH)					
(4) $BrCH_2CHBrO \rightarrow$ (11) $CH(O)Br$ + (23) CH_2Br	1.8	−2.1	−1.5	0.7	1.2
Pathway 3b					
(4) $BrCH_2CHBrO + O_2 \rightarrow$ (27) $BrCH_2C(O)Br + HO_2$	−29.6	−37.4	−38.3	−36.5	−37.3
(27) $BrCH_2C(O)Br + OH \rightarrow$ (28) $BrCHC(O)Br + H_2O$	−14.1	−20.8	−21.7	−23.5	−24.4
(28) $BrCHC(O)Br + O_2 \rightarrow$ (29) $BrCHO_2C(O)Br$	−13.3	−14.0	−16.2	−14.0	−16.0
(29) $BrCHO_2C(O)Br + NO \rightarrow$ (30) $BrCHOC(O)Br + NO_2$	−25.3	−24.2	−25.1	−16.7	−17.6
(30) $BrCHOC(O)Br + O_2 \rightarrow$ (31) $BrC(O)C(O)Br + HO_2$	−28.7	−35.7	−36.4	−34.7	−35.4
Pathway 3c (See 1b ΔH)					
(30) $BrCHOC(O)Br \rightarrow$ (14) $BrC(O)CH(O) + Br$	−14.5	−16.0	−14.6	−13.2	−12.0

[a] Species 10 optimization performed at B3LYP/6-31G(d).

$$(7)\ BrO_2CHCOH \rightarrow (8)\ HBrO_2CHCO \quad (9)$$

$$(7)\ BrO_2CHCH(O) + NO \rightarrow (12)\ BrOCHCHO + NO_2 \quad (10)$$

$$(7)\ BrO_2CHCH(O) \rightarrow (16)\ Br(HO_2)CCH(O) \quad (11)$$

Reaction 9 represents the isomerization of the BrO_2CHCOH (species 7) radical to the $HBrO_2CHCO$ (species 8) radical. This reaction takes place through a five-membered ring transition state, where the C−H−O vibration has a frequency of 3001*i* cm^{-1}. The barrier height is 20.7 kcal mol^{-1} and has an enthalpy of 3.3 kcal mol^{-1}. This reaction is the breakoff point for pathway 1a. Proceeding into pathway 1b, reaction 10 involves $BrCHO_2CH(O)$ (species 7) being reduced from a peroxy radical to an alkoxy radical. This reaction has an enthalpy of −15.9 kcal mol^{-1}. Reaction 11, the divergent reaction for pathway 1c and 1d, is another isomerization that involves a four membered ring transition state, having a vibrational mode of 2387*i* cm^{-1}. The activation energy and enthalpy are 43.0 and 0.5 kcal mol^{-1}, respectively. With a large activation energy and no beneficial enthalpy change, this pathway (reaction 11) is unfavorable.

Upon the formation of BrCHOCH(O) (species 12), pathway 2a diverges in two directions as shown in reactions 12 and 13

$$(12)\ BrOCHCHO \rightarrow (13)\ HCOCHO + Br \quad (12)$$

$$(12)\ BrOCHCHO + O_2 \rightarrow (14)\ BrC(O)CH(O) + HO_2 \quad (13)$$

The bromine extrusion in reaction 12 has an enthalpy change of −11.6 kcal mol^{-1}. A hydrogen abstraction occurs in reaction 13. The C−H−O vibration, with a 1524*i* cm^{-1} imaginary frequency corresponds to the transition state, with a barrier of 5.0 kcal mol^{-1}. The enthalpy is −36.9 kcal mol^{-1} and is related to the breaking of the C−H bond and formation of the O−H bond as well as the O−O double bond.

Pathway 1c proceeds from $BrC(HO_2)CH(O)$ (species 16) to form C(O)CH(O) (species 17) and HOBr (species 18) (reaction 14). However, a competing reaction exists as pathway 1d,

TABLE 2: Activation Energies for Oxidation Reactions of 1,2-Dibromoethane (kcal mol^{-1}) (Values Corrected with Zero Point Energy)

transition state	MP2 6-31G(d)	MP4 6-311++G (2d,2p)	MP4 6-311++G (2df,2p)	CCSD(T) 6-311++G (2d,2p)	CCSD(T) 6-311++G (2df,2p)
Initial Pathway					
[(1) $BrCH_2CH_2Br + OH \rightarrow$ (2) $BrCH_2CHBr + H_2O$]‡	7.3	4.2	3.4	2.7	1.9
Pathway 1a					
[(4) $BrCH_2CHBrO \rightarrow$ (5) $BrCH_2CH(O) + Br$]‡	5.4	2.2	2.4	−1.0	−0.9
[(5) $BrCH_2CH(O) + OH \rightarrow$ (6) $BrCHCH(O) + H_2O$]‡	11.3	6.6	5.8	4.1	3.3
[(7) $BrCHO_2CH(O) \rightarrow$ (8) $BrCH(HO_2)C(O)$]‡	25.8	22.0	21.7	21.1	20.7
Pathway 1b					
[(12) $BrCHOCH(O) + O_2 \rightarrow$ (14) $BrC(O)CH(O) + HO_2$]‡b	4.8	3.2	2.6	6.0	5.0
[(14) $BrC(O)CH(O) + OH \rightarrow$ (15) $BrC(O)C(O) + H_2O$]‡	11.7	5.6	5.0	1.0	0.6
Pathway 1c					
[(7) $BrCHO_2CH(O) \rightarrow$ (16) $BrC(HO_2)CH(O)$]‡	49.4	44.9	44.3	43.6	43.0
[(17) $C(O)CH(O) \rightarrow$ (19) $CH(O) + CO$]‡	5.4	2.1	3.6	2.3	3.8
Pathway 1d (See 1b TS)					
[(16) $BrC(HO_2)CH(O) \rightarrow$ (14) $BrC(O)CH(O) + OH$]‡	9.3	4.5	5.4	−2.8	−1.9
Pathway 2a					
[(4) $BrCH_2CHBrO \rightarrow$ (5) $BrCH_2CH(O) + Br$]‡	5.4	2.2	2.4	−1.0	−0.9
[(5) $BrCH_2CH(O) + OH \rightarrow$ (20) $BrCH_2C(O) + H_2O$]‡	6.6	2.2	1.6	−1.5	−2.0
[(22) $BrCH_2C(O)O \rightarrow$ (23) $CH_2Br + CO_2$]‡	6.1	4.5	3.5	2.0	0.8
[(25) $CH_2BrO \rightarrow$ (26) $CH_2(O) + Br$]‡	8.8	5.6	5.8	2.1	2.2
[(25) $CH_2BrO + O_2 \rightarrow$ (11) $CH(O)Br + HO_2$]‡	7.0	3.1	1.4	4.2	2.8
Pathway 2b (See 2a TS)					
[(20) $BrCH_2C(O) \rightarrow$ (23) $CH_2Br + CO$]‡	15.5	11.2	12.8	10.3	11.7
Pathway 3a (See 2a TS)					
[(4) $BrCH_2CHBrO \rightarrow$ (11) $CH(O)Br$ + (23) CH_2Br]‡	17.8	13.0	12.8	11.5	11.3
Pathway 3b					
[(4) $BrCH_2CHBrO + O_2 \rightarrow$ (27) $BrCH_2C(O)Br + HO_2$]‡	2.9	−0.8	−2.5	1.8	0.5
[(27) $BrCH_2C(O)Br + OH \rightarrow$ (28) $BrCHC(O)Br + H_2O$]‡	9.8	6.5	5.5	4.4	3.5
[(30) $BrCHOC(O)Br + O_2 \rightarrow$ (31) $BrC(O)C(O)Br + HO_2$]‡	1.1	−2.8	−4.4	0.1	−1.1
Pathway 3c (See 1b TS)					
[(30) $BrCHOC(O)Br \rightarrow$ (14) $BrC(O)CH(O) + Br$]‡	5.1	3.5	3.8	−0.5	−0.3

with the conversion of $BrC(HO_2)CH(O)$ (species 16) to $BrC(O)CH(O)$ (species 14) (reaction 15)

$$(16)\ Br(HO_2)CCH(O) \rightarrow (17)\ (O)CCH(O) + (18)\ HOBr \quad (14)$$

$$(16)\ Br(HO_2)CCH(O) \rightarrow (14)\ BrC(O)CH(O) + OH \quad (15)$$

Reaction 14, a unimolecular fragmentation has an enthalpy change of -16.6 kcal mol^{-1}. The hydroxyl radical extrusion, in reaction 15, has a transition state vibrational frequency of $1379i$ cm^{-1}, and the associated activation energy and enthalpy are -1.9 and -36.1 kcal mol^{-1}, respectively.

3.3.3. Pathway 2. The potential energy surface for pathway 2 is shown in Figure 5c. This pathway branches from pathway 1 with $BrCH_2CH(O)$ (species 5) via a hydrogen abstraction to form $BrCH_2C(O)$ (species 20). Immediately following this abstraction, two possible reactions emerge (reactions 16 and 17)

$$(20)\ BrCH_2CO + O_2 \rightarrow (21)\ BrCH_2COO_2 \quad (16)$$

$$(20)\ BrCH_2CO \rightarrow (23)\ CH_2Br + CO \quad (17)$$

Reaction 16, the starting point for pathway 2a, depicts the addition of molecular oxygen forming a peroxy radical. The enthalpy of this reaction is -32.3 kcal mol^{-1}, corresponding to the formation of the C$-$O bond. The fragmentation in reaction 17 is the starting point for pathway 2b. It has an enthalpy of 1.6 kcal mol^{-1}. The transition state of this reaction has an energetic barrier of 11.7 kcal mol^{-1} and a vibrational mode of $553i$ cm^{-1} associated with the C$-$C bond stretch.

After progressing two more steps, a reduction by NO and the extrusion of a CO_2 molecule, pathway 2a converges with the pathway 2b at CH_2Br (species 23). The pathway continues on two more steps until reaching a final diverging step. Reactions 18 and 19 listed below show the two possible final steps of pathway 2

$$(25)\ BrCH_2O \rightarrow (26)\ CH_2(O) + Br \quad (18)$$

$$(25)\ BrCH_2O + O_2 \rightarrow (11)\ CH(O)Br + HO_2 \quad (19)$$

The bromine extrusion of reaction 18 has an activation energy of 2.2 kcal mol^{-1}. Representing this transition state is the vibrational frequency at $623i$ cm^{-1}. The breaking of the C$-$Br bond and forming of the C$-$O double bond has an enthalpy of -7.8 kcal mol^{-1}. In reaction 19, molecular oxygen oxidizes CH_2BrO (species 25) by removing the hydrogen atom to form HO_2 and a final product of CH(O)Br (species 11). The enthalpy associated with this process is -35.2 kcal mol^{-1}, with an activation energy of 2.8 kcal mol^{-1}. The transition state corresponds to the C$-$H$-$O vibration and has a vibrational mode frequency of 1397i cm^{-1}.

3.3.4. Pathway 3. Figure 5d represents the potential energy surface for pathway 3. As noted earlier this pathway breaks off at $BrCH_2CHBrO$ (species 4). The initial step of pathway 3a forms CH_2Br (species 23). The continuation of pathway 3a follows the same as that of pathway 2. The split between 3b and 3c occurs with the two possible reactions listed below (reactions 20 and 21)

$$(30)\ BrOCHCOBr + O_2 \rightarrow (31)\ BrCOCOBr + HO_2 \quad (20)$$

$$(30)\ BrOCHCOBr \rightarrow (14)\ BrCOCOH + Br \quad (21)$$

Another hydrogen abstraction is seen in reaction 20. This transition state has a vibrational frequency mode similar to reaction 19 at $1557i$ cm^{-1}. The activation barrier and enthalpy are -1.1 and -35.4 kcal mol^{-1}. Reaction 21 represents a bromine extrusion with activation energy and enthalpy of -0.3 and -12.0 kcal mol^{-1}. Finally, the C$-$Br stretch associated with the negative frequency, and thus correlated with the transition state, is $672i$ cm^{-1}.

4. Atmospheric Implications

Halogenated compounds are known to deplete ozone through their release of halogen radicals.[1−3] Bromine in particular will catalyze the destruction of ozone 40−50 times more effectively than chlorine atoms.[13−17] However, halogenated compounds considered VSL are viewed as benign with respect to ozone depletion. VSL compounds are thought to have short lifetimes, but the halogenated products they produce may have lifetimes long enough to be transported to the stratosphere and therefore have the ability to deplete ozone. Additionally, studies have shown a number of VSL compounds to be present in the upper troposphere and the lower stratosphere, indicating their lifetimes may be longer than previously thought. Specifically, dibromoethane has been measured at 1.1 ppt of bromine in these areas.[11] All these factors make the atmospheric oxidation products of dibromoethane of particular concern.

From all pathways discussed, the degredation of dibromoethane results in the following products: OH, CO, CO_2, Br radicals, CH(O)Br (species 11), CH(O)CH(O) (species 13), HOBr (species 18), $CH_2(O)$ (species 26), and BrC(O)C(O)Br (species 31). Because of the complexity of the EDB degradation, favorable pathways as well as predicted product ratios are not given. These predictions require the consideration of all kinetic properties for each reaction as well as the incorporation of atmospheric conditions, including reactant concentrations. Nevertheless, the information from this work provides necessary parameters to estimate kinetic rate data to assist in this assessment.

The products discussed above highlight the significant environmental problems associated with dibromoethane. Bromine-containing compounds produced from the dibromoethane degradation may have long lifetimes, allowing transport into the stratosphere. In the stratosphere, these compounds will undergo further oxidation or photolysis, eventually releasing bromine radicals with the ability to catalyze the destruction of ozone. Bromine containing compounds produced from the EDB reaction include CH(O)Br, HOBr, and Br(O)CC(O)Br. A literature search shows that no studies have indicated any known atmospheric source of Br(O)CC(O)Br, as such this product is of particular interest.

To better understand the resulting product ratios, and ultimately the ability of products resulting from the EDB atmospheric oxidation to deplete ozone, atmospheric modeling should be employed. Weubbles et al.[51] determined the ozone depletion potential of 1-bromopropane using a computational atmospheric modeling program. This program allows for an estimate of a compounds ability to deplete ozone based upon the reactions involved in the degradation, lifetimes of the oxidation products, transport times, as well as the influence of other atmospheric reactions. These parameters are accounted for according to global location, time of year, and time of day. By use of the atmospheric oxidation mechanism presented here, a full atmospheric model of EDB would allow for an optimum understanding of the impact of EDB on stratospheric ozone depletion.

Acknowledgment. The authors express thanks to the U.S. Department of Energy Global Change Education Program for financial support through the Graduate Research Environmental Fellowship awarded to Carrie J. Christiansen.

Supporting Information Available: Zero point corrected energies and vibrational frequencies of all species are available as supplementary tables. This information is available free of charge via the Internet at http://pubs.acs.org.

References and Notes

(1) Molina, M. J.; Rowland, F. S. *Nature* **1974**, *249*, 810.
(2) Rowland, F. S. *Angew. Chem., Int. Ed.* **1996**, *35*, 1786.
(3) Cohn, J. P. *BioScience* **1987**, *37*, 647.
(4) Finlayson-Pitts, B. J.; Pitts, J. N. Chemistry of the Upper and Lower Atmosphere; Academic Press: 2000.
(5) Rowland, F. S.; Molina, M. J. *Rev. Geophys. Space Ge.* **1975**, *13*, 1.
(6) Watson, R. T.; Sander, S. P.; Yung, Y. L. *J. Phys. Chem.* **1979**, *83*, 2936.
(7) Wofsy, S. C.; McElroy, M. B.; Yung, Y. L. *Geophys. Res. Lett.* **1975**, *2*, 215.
(8) Yu, X.; Ichihara, G.; Kitoh, J.; Xie, Z.; Shibata, E.; Kamijima, M.; Asaeda, N.; Takeuchi, Y. *J. Occup. Health* **1998**, *40*, 234.
(9) Wuebbles, D. J.; Jain, A. K.; Patten, K. O.; Connell, P. S. *Atmos. Environ.* **1997**, *32*, 107.
(10) Levine, J. G.; Braesicke, P.; Harris, N. R. P.; Savage, N. H.; Pyle, J. A. *J. Geophys. Res.* **2007**, *112*, 1.
(11) Sturges, W. T.; Worton, D. R.; O'Sullivan, D. A.; Engel, A.; Laube, J. *J. Geophys. Res. Abstracts* **2007**, *9*, 10792.
(12) Ko, M. K. W.; Poulet, G. *Scientific Assessment of Ozone Depletion* **2002**, 2002.
(13) Dixon, D. A.; Jong, W. A. D.; Peterson, K. A.; Francisco, J. S. *J. Phys. Chem. A* **2002**, *106*, 4725.
(14) Scientific Assessment of Stratospheric Ozone,1989.
(15) Daniel, J. S.; Solomon, S.; Portmann, R. W.; Garcia, R. R. *J. Geophys. Res.* **1999**, *104*, 23871.
(16) Kamboures, M. A.; Hansen, J. C.; Francisco, J. S. *Chem. Phys. Lett.* **2002**, *353*, 335.
(17) Anderson, J. G.; Brune, W. H.; Lloyd, S. A.; Toohey, D. W.; Sander, S. P.; Starr, W. L.; Loewenstein, M.; Podolske, J. R. *J. Geophys. Res.* **1989**, *94*, 11480.
(18) Koga, M.; Hanada, Y.; Zhu, J.; Nagafuchi, O. *Microchem. J.* **2001**, *68*, 257.
(19) Clark, A. I.; McIntyre, A. E.; Perry, R.; Lester, J. N. *Environ. Pollut.* **1984**, *7*, 141.
(20) Srivastava, A.; Joseph, A. E.; Devotta, S. *Atmos. Environ.* **2006**, *40*, 892.
(21) Pankow, J. F.; Luo, W.; Isabelle, L. M.; Bender, D. A.; Baker, R. *J. Anal. Chem.* **1998**, *70*, 5213.
(22) Singh, H. B.; Salas, L.; Viezee, W.; Sitton, B.; Ferek, R. *Atomos. Environ.* **1992**, *26A*, 2929.
(23) Fischer, R.; Weller, R.; Jacobi, H.; Ballschmiter, K. *Chemosphere* **2002**, *48*, 981.
(24) Class, T.; Kohnle, R.; Ballschmiter, K. *Chemosphere* **1986**, *15*, 429.
(25) Bravo, A. H.; Sanchez, A. P.; Sosa, E. R.; Keener, T. C.; Lu, M. *Clean Technol. Environ. Policy* **2006**, *8*, 174.
(26) Status of Pesticides in Registration and Special Review; United States Environmental Protection Agency,1998.
(27) Stirling, G. R.; Nikulin, A. *Aust. Plant. Pathol.* **1998**, *27*, 234.
(28) Class, T.; Ballschmiter, K. *J. Atmos. Chem.* **1988**, *6*, 35.
(29) Laturnus, F. *Chemosphere* **1995**, *31*, 3387.
(30) Laturnus, F.; Wiencke, C.; Kloeser, H. *Mar. Environ. Res.* **1996**, *41*, 169.
(31) Laturnus, F. *Mar. Chem.* **1996**, *55*, 359.
(32) Castro, C. E. *Environ. Toxicol. Chem.* **1993**, *12*, 1609.
(33) Deckard, L. A.; Willis, J. C.; Rivers, D. B. *Biotechnol. Lett.* **1994**, *16*, 1221.
(34) Ethylene dibromide US Environmental Protection Agency Ecological Toxicity Database (ECOTOX); United States Environmental Protection Agency,1998.
(35) Budavari, S.; O'Neil, M. J.; Smith, A.; Heckelman, P. E. The Merck Index, 12th ed.; 1996.
(36) Domagalski, J. L.; Dubrovsky, N. M. *J. Hydrol.* **1992**, *130*, 299.
(37) *CRC Handbook of Chemistry and Physics*, 88th ed.; CRC Press: Boca Raton, FL, 2007.
(38) Torkelson, T. R. *Patty's industrial hygiene and toxicology*, 4th ed.; Wiley: New York, 1994; Vol. 2.
(39) Brown, C. W.; Zhou, A. *J. Appl. Spectrosc.* **2001**, *55*, 44.
(40) Bose, P. K.; Henderson, D. O.; Ewig, C. S.; Polavarapu, P. L. *J. Phys. Chem.* **1989**, *93*, 5070.
(41) Atkinson, R. *Chem. Rev.* **1985**, *85*, 69.
(42) Qiu, L. X.; Shi, S. H.; Xing, S. B.; Chen, X. G. *J. Phys. Chem.* **1992**, *96*, 685.
(43) Howard, C. J.; Evenson, K. M. *J. Chem. Phys.* **1976**, *64*, 197.
(44) Frisch, M. J.; Trucks, G. W.; Schlegel, H. B.; Scuseria, G. E.; Robb, M. A.; Cheeseman, J. R.; Montgomery, J.; Vreven, T.; Kudin, K. N.; Burant, J. C.; Millam, J. M.; Iyengar, S. S.; Tomasi, J.; Barone, V.; Mennucci, B.; Cossi, M.; Scalmani, G.; Rega, N.; Petersson, G. A.; Nakatsuji, H.; Hada, M.; Ehara, M.; Toyota, K.; Fukuda, R.; Hasegawa, J.; Ishida, M.; Nakajima, T.; Honda, Y.; Kitao, O.; Nakai, H.; Klene, M.; Li, X.; Knox, J. E.; Hratchian, H. P.; Cross, J. B.; Adamo, C.; Jaramillo, J.; Gomperts, R.; Stratmann, R. E.; Yazyev, O.; Austin, A. J.; Cammi, R.; Pomelli, C.; Ochterski, J. W.; Ayala, P. Y.; Morokuma, K.; Voth, G. A.; Salvador, P.; Dannenberg, J. J.; Zakrzewski, V. G.; Dapprich, S.; Daniels, A. D.; Strain, M. C.; Farkas, O.; Malick, D. K.; Rabuck, A. D.; Raghavachari, K.; Foresman, J. B.; Ortiz, J. V.; Cui, Q.; Baboul, A. G.; Clifford, S.; Cioslowski, J.; Stefanov, B. B.; Liu, G.; Liashenko, A.; Piskorz, P.; Komaromi, I.; Martin, R. L.; Fox, D. J.; Keith, T.; Al-Laham, M. A.; Peng, C. Y.; Nanayakkara, A.; Challacombe, M.; Gill, P. M. W.; Johnson, B.; Chen, W.; Wong, M. W.; Gonzalez, C.; Pople, J. A. Gaussian 03, revision B.03; Gaussian Inc.: Pittsburgh, PA, 2003.
(45) Martínez-Avilés, M.; Rosado-Reyes, C. M.; Francisco, J. S. *J. Phys. Chem. A* **2007**, *111*, 11652.
(46) Chandra, A. K.; Uchimaru, T. *J. Comput. Chem.* **2001**, *22*, 1509.
(47) Zelek, S.; Wasilewski, J.; Heldt, *J. Comput. Chem.* **2000**, *24*, 263.
(48) Kroll, J. H.; Ng, N. L.; Murphy, S. M.; Varutbangkul, V.; Flagan, R. C.; Seinfeld, J. H. *J. Geophys. Res.* **2005**, *110*, D23207.
(49) Liggio, J.; Li, S.-M.; McLaren, R. *J. Geophys. Res.* **2005**, *110*, D10304.
(50) Tadic, J.; Moortgat, G. K.; Wirtz, K. *J. Photochem. Photobiol. A* **2006**, *117*, 116.
(51) Wuebbles, D. J.; Jain, A. K.; Patten, K. O.; Connell, P. S. *Atmos. Environ.* **1998**, *32*, 107.

JP807966P